

***Scientific report on the project implementation in the period January 2012 –  
December 2016***

The main results obtained during this contract in 2016 can be summarized as it follows.

***A. Temperature control of crystalline status and phenomenological modes***, applications to TiO<sub>2</sub> versus Ti layers T. ROSCA, S. BAZGAN, G. DORCIOMAN, C. RISTOSCU, G. POPESCU-PELIN, N. ENAKI, I. N. MIHAILESCU, Romanian Reports in Physics, Vol. 68, No. 1, P. 241–248, 2016

In this work we propose a phenomenological model of the phase transition from the crystalline to amorphous one in the deposition of TiO<sub>2</sub> or Ti onto Si or SiO<sub>2</sub> substrate. The molecular modeling study of the adsorption of protein subdomains with unlike secondary structures on the surfaces of ceramic titanium dioxide (TiO<sub>2</sub>), forming a passivating film on titanium bio-materials that provides the interface between the bulk metal and the physiological environment depends on the deposition structure of this material on the substrate and performance.

In this paper a special attention is devoted to the titanium films deposited in two phases: crystalline and amorphous, necessary for the controlled adhesion of the organic molecules.

It is supposed that the electrons on the Si surface are coupled due to existence of voids in the crystalline continuity and have a smaller coupling energy than the electrons forming covalent bonds between Si atoms of the crystalline substrate. Correspondingly, the coupled energy can be easily dropped by the Ti atoms relaxing on this surface. When the TiO<sub>2</sub> radicals get closer to surface, the unpaired electrons can break the weak coupled pairs of electrons from the surface bounds so that Si crystalline lattice is growing with Ti material. This is possible due to the fact that the coupled electrons to the substrate surface of Si reach a more stable state when entering into a new electronic bond (covalent or ionic) with TiO<sub>2</sub>. Thus, the surface starts to be arranged as a new crystal lattice of TiO<sub>2</sub>.

In order to describe the phase transition from crystalline to amorphous we represent the stable chemical bonds between the  $\alpha$ -atoms by the crystalline harmonic potential:

$$V = \sum_{\alpha} \frac{k(x_{\alpha}^0 - x_{\alpha})^2}{2} \quad (1)$$

where  $x_{\alpha}^0$  is the equilibrium position of the  $\alpha$  atom of Si placed on surface coupled with the Ti atom, while  $x_{\alpha}^0 - x_{\alpha}$  is the deviation from the equilibrium position of the Ti atom which enters into the chemical bond with the  $\alpha$  Si atom.

This potential energy represents the stable crystalline bounds between the Ti and Si atoms and is described by a parabolic function of N variables. When increasing the temperature, the collective oscillations of Ti atoms on the surface bounds become non-harmonic. In excess of a critical temperature, the crystalline arrangement of the atoms on the Si inner surface becomes instable. Beginning with this temperature, the collective potential in Eq. (1) has the big number of other nonregular equilibrium states, characteristic to the non-crystalline deposition on the Si substrate.

A simple nonlinear potential having two minima can be inferred by decomposing the interaction energy at the position displacement of  $\alpha$  Ti atom,  $u_\alpha = x_\alpha^0 - x_\alpha$  and has the following form:

$$V = \sum_\alpha \frac{k(x_\alpha^0 - x_\alpha)^2}{2} - \sum_\alpha \beta(x_\alpha^0 - x_\alpha)^4 + \sum_\alpha \gamma(x_\alpha^0 - x_\alpha)^6 \quad (2)$$

where  $\alpha$ ,  $\beta$  and  $\gamma$  are the constants of the non-Harmonic potential. These constants should be determined from the experiments where is studied the transition from the crystalline to amorphous phases of the deposited material when increasing the temperature.

To simplify this approach we consider the potential energy of only one center in the material:

$$V(x_\alpha^0 - x_\alpha) = \frac{k(x_\alpha^0 - x_\alpha)^2}{2} - \beta(x_\alpha^0 - x_\alpha)^4 + \gamma(x_\alpha^0 - x_\alpha)^6 \quad (3)$$

In the expression above the harmonic constant  $k$  describes the crystalline phase of the deposited

material on the substrate and can be determined by the dispersion law of the acoustic vibrations on the interface between the Si and Ti. For a temperature below the critical one the connection

between the elastic constant  $k$  and the sound velocity in the material is given by  $v_s = \sqrt{\frac{k}{m}}$ , where  $m$  is the reduced mass of the coupled system Ti-Si.

The potential energy given by Eqn. 3 is represented graphical in Fig. 1 for two different sets of quantities  $\alpha, \beta, \gamma$ .

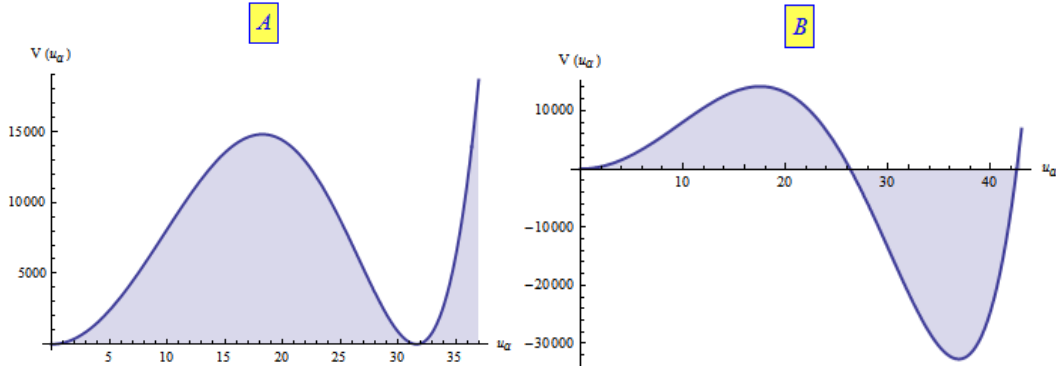


Fig. 1 – Glass minima of non-harmonic potential  $V(u)$  for following parameters of the system:  
 A.  $k/2 = 100$ ,  $\beta = 0.2$  and  $\gamma = 0.0001$ ; B.  $k/2 = 100$ ,  $\beta = 0.2$  and  $\gamma = 0.00008$ .

From this figure it is observed that the function  $V(u_\alpha) = \frac{k(u_\alpha)^2}{2} - \beta(u_\alpha)^4 + \gamma(u_\alpha)^6$  starts from zero for  $u_\alpha = 0$ , is increasing to a maximum value  $u_{\max}$  after which is decreasing to a minima for  $u_{\min}$ . After reaching the minimum value at the critical point, the non-harmonic potential increases again. The second minimum corresponds to the glass deposition of the TiO<sub>2</sub> material on the substrate.

Next, we studied the connection of these parameters with thermodynamic functions of the material near the critical point of phase transition. For this, we revised the second order phase

transition in the critical point  $2\beta = \sqrt{\frac{3\gamma k}{2}}$  starting from which the second “glass” minimum of potential function is possible. According to the theory of the second order phase transition, one can find the connection between the parameters  $\beta$  and  $\gamma$  using the decomposition of the thermodynamic potential near the critical point  $2\beta = \sqrt{\frac{3\gamma k}{2}}$ . We will use near this point the new variable  $X^2 = u^2 - u_m^2$ , where  $u_m = u_{\max} = u_{\min} = \sqrt{\frac{2\beta}{3\gamma}}$  at the critical point  $T=T_c$ . Starting with this temperature, the deposition passes from crystalline to vitreous (glass) phases described mathematically by the appearance of the second well of the potential.

The problem is reduced to the second order phenomenological theory of the phase transition. The thermodynamic potential can be decomposed in similar series near the critical point  $T = T_c$ :

$$\Phi(T, P, X) = \Phi_0 + A(P, T)X^2 + B(P, T)X^4 \quad (4)$$

Correspondingly, one can suggest that the parameter  $A(P, T)$  don't have singular points close to the phase transition and can be represented as a linear function of the displacement from critical temperature  $A(P, T) = a(P)(T - T_c)$ . The coefficient  $B(P, T)$  can be approximated by its value in the critical point  $B(P, T_c)$ . After this approximation, the thermodynamic potential close to the vicinity of the critical point is described by the following temperature dependence  $B(P, T_c)$ :

$$\Phi(T, P, X) = \Phi_0 + a(P)(T - T_c)X^2 + B(P, T_c)X^4 \quad (5)$$

Close to the vicinity of the second order phase transition, the critical temperature is described by the extremes of the function:  $\frac{\partial \Phi(T, P, X)}{\partial X} = 0$ . By neglecting the higher order decompositions on the new function  $X^2$  we obtain the following expression for the entropy of the system:

$$S = S_0 + \frac{a^2}{2B}(T_c - T) \quad (6)$$

In a similar way, one can obtain the following expression of specific heat capacity of the deposited material:

$$C_p = C_{p0} - \theta(T - T_c) \frac{a^2}{2B} \quad (7)$$

From the specific heat capacity jump at critical point, , one can infer the parameters  $\gamma_c$  and  $\beta_c$ . It is supposed that  $B = \beta$ . To find the dependence of the coefficient  $a^2$  on the  $\gamma$  and  $\beta$  non-harmonic parameter we use the following equation:

$$A = \frac{k}{2} - 2u_m^2\beta + 3\gamma u_m^4 = a(T_c - T) \quad (8)$$

Setting the equation  $\frac{k}{2} - 2u_m^2\beta + 3\gamma u_m^4 = 0$  we find the solutions  $u_{m2}^2$  and  $u_{max}^2$  and we can factorize the LHS to  $3\gamma(u_m^2 - u_{m2}^2)(u_m^2 - u_{max}^2)$ . This thing let us to obtain the following equation:

$$\left(\frac{2\beta}{3\gamma}\right)^2 - \frac{k}{6\gamma} = -\frac{a(T_c - T)}{3\gamma} \quad (9)$$

Based upon critical temperature and the jump of the specific heat at the critical temperature we can assume that  $\beta = \beta_0 T$  and simplify Eqn. 9 to :

$$\left(\frac{2\beta_0}{3\gamma}\right)^2 (T^2 - T_c^2) = -\frac{a(T_c - T)}{3\gamma} \quad (10)$$

Or more simplified:

$$\left(\frac{2\beta_0}{3\gamma}\right)^2 (T + T_c) = \frac{a}{3\gamma} \quad (11)$$

This equation permits us to find the values of  $\gamma_c$ ,  $\beta_c$  and  $T_c$  at  $T=T_c$ ,  $\beta_0 = \beta_0 T$  and  $\gamma=\gamma_c$ :

$$T_c^2 = \frac{3\gamma k}{8\beta_0^2}, \quad \beta_c^2 = \frac{3\gamma k}{8}, \quad \gamma_c = \frac{8\beta_c^2}{3aT_c} \quad (12)$$

The phenomenological approach allows finding the connection between experimental observations and theoretical predictions. For example, the distance between first and the second minima of double hole potential can be related to the mean size of the disorder in glasses phase deposition of the TiO2 material on Si or SiO2 substrates.

**B.** “The temperature field distributions in a Fe target under low power laser irradiation and low heat transfer coefficient conditions: experiments versus simulations”, A. BUCĂ, V. DAMIAN, M. OANE, R. V. MEDIANU, I. N. MIHĂILESCU, G. POPESCU-PELIN, OPTOELECTRONICS AND ADVANCED MATERIALS – RAPID COMMUNICATIONS Vol. 10, Iss. 1 - 2, January - February 2016, p. 29 – 31

In this section we present a new approach to elaborate a laser-metal thermal interaction model with consideration of solving instead the two temperatures model (TTM): electron and phonon temperatures equations, just one common Fourier equation. Because the power of laser beam is low and the heat transfer coefficients are low we may consider using two temperatures model that: the electron temperature is equal with phonon temperature. In this situation we may use only one heat Fourier equation. Experimental data versus simulations are also presented.

The two temperature model was discovered by the Russian school of theoretical physics almost 35 years ago. The solutions of the TTM can get from solving two coupled differential equations. In our special situation, in which we have: low power irradiation and low transfer coefficient, the TTM reduces to Fourier model.

Using the integral transform technique we have the solution (using the notations from references [3, 4]):

$$T_e = \sum_{i=1}^{\infty} \sum_{j=1}^{\infty} \sum_{k=1}^{\infty} I_1(\lambda_i, \mu_j, \xi_k) \cdot I_2(\lambda_i, \mu_j, \xi_k, t) \cdot K_x(\lambda_i, x) \cdot K_y(\mu_j, y) \cdot K_z(\xi_k, z) \quad (1)$$

If we take into account just the first 10 terms (for  $i, j, k$ ) we obtain an analytical solution:

$$T_e = \sum_{i=1}^{10} \sum_{j=1}^{10} \sum_{k=1}^{10} I_1(\lambda_i, \mu_j, \xi_k) \cdot I_2(\lambda_i, \mu_j, \xi_k, t) \cdot K_x(\lambda_i, x) \cdot K_y(\mu_j, y) \cdot K_z(\xi_k, z) \quad (2)$$

Here:

$$I_1(\lambda_i, \mu_j, \xi_k) = \frac{1}{KC_i C_j C_k} \int_0^a \int_0^b \int_0^c P_a(\vec{r}, t) \cdot K_x(\lambda_i, x) \cdot K_y(\mu_j, y) \cdot K_z(\xi_k, z) \quad (3)$$

and

$$I_2(\lambda_i, \mu_j, \xi_k, t) = \frac{1}{\lambda_i^2 + \mu_j^2 + \xi_k^2} \left[ 1 - e^{\gamma_{ijk}^2 \cdot t} - \left( 1 - e^{-\gamma_{ijk}^2 (t-t_0)} \right) \cdot H(t-t_0) \right] \quad (4)$$

Where

$$\gamma_{ijk}^2 = \gamma(\lambda_i^2 + \mu_j^2 + \xi_k^2) \quad (5)$$

$P_a$  represents the absorbed power.  $C_i, C_j, C_k$  are the normalizing constants [3-6]. We have 3 differential equations from traditional theory [3, 4] ( $K$  –represents the eigen-functions,  $\lambda, \mu, \xi$  the eigen-values):

$$\frac{\partial^2 K_x}{\partial x^2} + \lambda_i^2 K_x = 0 \quad ; \quad \frac{\partial^2 K_y}{\partial y^2} + \mu_j^2 K_y = 0 \quad (6)$$

We have in general three types of heat transfer by: i) radiation, ii) convection and iii) conduction. In our case the heat lost by conduction is not neglected as the sample is fixed on a plastic support. The heat rate lost by radiation may be written  $\sigma \cdot E \cdot (T^4 - T_0^4)$ , which in linear approximation is given by  $4\sigma \cdot T_0^3 \cdot E \cdot (T - T_0) \equiv h_{rad} \cdot (T - T_0)$ . Here  $h_{rad} = 4 \cdot \sigma \cdot T_0^3 \cdot E$ , where  $T_0 = 298K$ ,  $\sigma = 5.6 \times 10^{-8} W m^{-2} K^{-4}$  is the Stephan Boltzmann constant, and  $E$  is the thermal emissivity which for polished metallic surfaces can be taken 0.05. We obtain  $h_{rad} = 3 \cdot 10^{-7} W mm^{-2} K^{-1}$ . The heat rate loss by convection when the sample is in air obeys a power law given by  $20 \cdot 10^{-9} (T - T_0)^{5/4} [W mm^{-2}]$  [13]. This expression can be further linearized:

$20 \cdot 10^{-9} (T - T_0)^{1/4} (T - T_0) [W mm^{-2}] = h_{conv} \cdot (T - T_0) [W mm^{-2}]$ . In consequence we can conclude:  $h_{conv} \cong 0.8 \cdot 10^{-7} W mm^{-2} K^{-1}$ , where we have considered:  $T - T_0 = 300K$ . The total heat transfer coefficient is:  $h_{total} = h_{rad} + h_{conv} \cong 3.8 \cdot 10^{-7} W mm^{-2} K^{-1}$ , which corresponds to the sample surrounded by air. For a sample fixed on a plastic support:  $h_{total} = h_{rad} \cong 3 \cdot 10^{-7} W mm^{-2} K^{-1}$ .

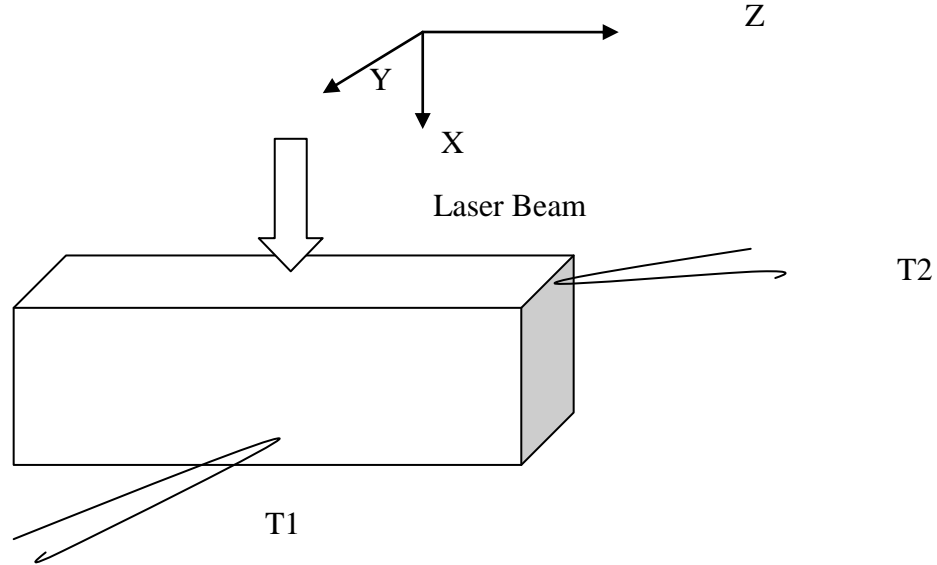


Fig.2. The experimental set-up

Table 1: The experimental values on faces 1 and 2 of the Fe target under laser irradiation with a laser with fluence of  $7 J/cm^2$

	1	2	3	4	5	
N o. pulses	100	150	200	300	500	ulses
F luence	6.9	6.9	7	7	7	/cm <sup>2</sup>

<b>T<sub>empT1</sub></b>	5.3	5.6	5.5	5.8	5.5	5.8	5.7	6.5	5.8	6.8	<b>°C</b>
<b>te<sub>mpT2</sub></b>	5.5	5.7	5.7	6.1	5.7	6.1	5.8	6.6	5.9	7.2	<b>°C</b>
<b>T1</b> □		.3		.3		.3		.8			<b>°C</b>
<b>T2</b> □		.2		.4		.4		.8		.3	<b>°C</b>

Table 2: The experimental values on faces 1 and 2 of the Fe target under laser irradiation with a laser with fluence of 47 J/cm<sup>2</sup>

	<b>1</b>	<b>2</b>	<b>3</b>	<b>4</b>	<b>5</b>						
<b>N<sub>o. pulses</sub></b>	<b>100</b>	<b>150</b>	<b>200</b>	<b>300</b>	<b>500</b>	<b>ulses</b>					
<b>F<sub>luence</sub></b>	<b>46.7</b>	<b>46.7</b>	<b>5</b>	<b>47.0</b>	<b>47.0</b>	<b>47.0</b> <b>/cm<sup>2</sup></b>					
<b>T<sub>empT1</sub></b>	6.8	7.1	6.9	7.5	7.1	7.7	7.1	8.1	7.2	8.8	<b>°C</b>
<b>te<sub>mpT2</sub></b>	6.8	7.3	7	7.7	7.1	8	7.2	8.5	7.2	9.5	<b>°C</b>
<b>T1</b> □		.3		.6		.6				.6	<b>C</b>
<b>T2</b> □		.5		.7		.9		.3		.3	<b>°C</b>

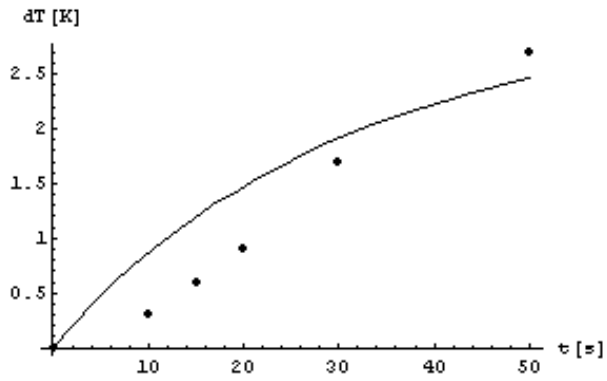


Fig. 3. The experimental points versus simulated temperature fields (continuous line) for T1 and a fluence of  $7 \text{ J/cm}^2$

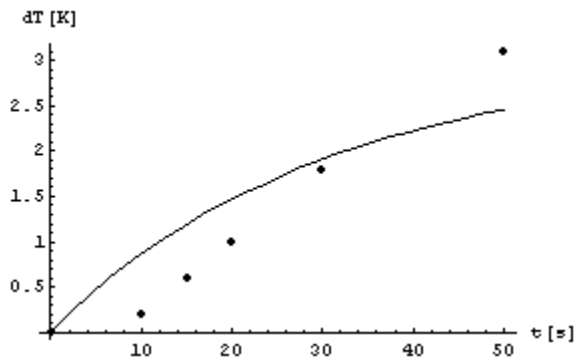


Fig. 4. The experimental points versus simulated temperature fields (continuous line) for T2 and a fluence of  $7 \text{ J/cm}^2$ .

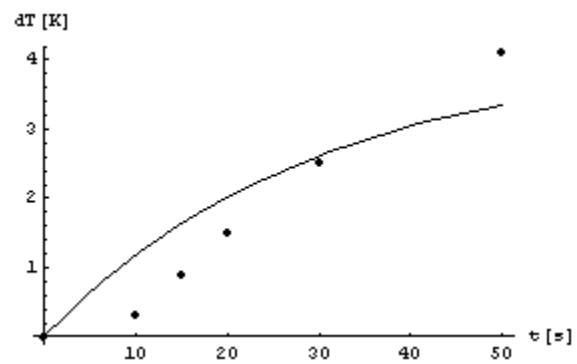


Fig. 5. The experimental points versus simulated temperature fields (continuous line) for T1 and a fluence of  $47 \text{ J/cm}^2$

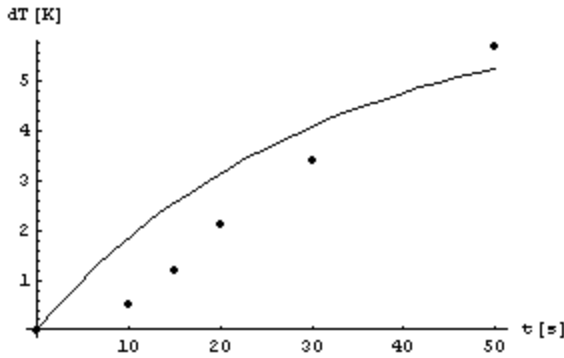


Fig. 6. The experimental points versus simulated temperature fields (continuous line) for T2 and a fluence of 47 J/cm

We have a 1cm x 1 cm x 1cm Fe target. Like heating source we have used a Nd:YAG laser working on his third harmonic at 355 nm (Continuum – Surelite II). The laser has a pulse length at FWHM of 5ns, with a repetition frequency of 10 Hz and a beam divergence of 0.6 mrad.

We have obtained a simple solution for the two model temperature. The solution can help to know the thermal effect in laser-metal interaction. Our conclusion regarding the fit between experimental data and theoretical simulations is that we have a good agreement between them. In fact it is the same kind of experiments and simulations like in references with the only difference that now we have photons instead of electrons.

C. The main original results obtained during the whole period of this contract were summarized in the book chapter entitled “*Pulse laser deposited TiO<sub>2</sub> based films: Synthesis, electronic structures and photocatalytic activity*”, Oksana Linnik, Nataliia Chorna, Nataliia Smirnova, Anna Eremenko, Oleksandr Korduban, Nicolaie Stefan, Carmen Ristoscu, Gabriel Socol, Marimona Miroiu, Ion N. Mihailescu, Chapter 5 in “*Semiconductor Photocatalysis - Materials, Mechanisms and Applications*”, InTech, Ed. Wenbin Cao, ISBN 978-953-51-2483-2 (2016) pp. 135-161.

An appropriate selection of gas mixture, pressure, and temperature during PLD synthesis is identified for the optimum photocatalytic activity of semiconductive materials.

The highest photocatalytic conversion yields in the dichromate ions reduction are obtained for nitrogen-doped 10% ZrO<sub>2</sub>/TiO<sub>2</sub> synthesized in N<sub>2</sub>:CH<sub>4</sub> = 5:1 at 100 Pa and at 450°C under both UV and visible light. This is the result of effective nitrogen atom substitution into titania lattice as confirmed by N1s XPS line at 395.8 eV. When the films were synthesized at low pressure of 3 Pa, the only Ns peak with the binding energy 395.8 eV was observed and photocatalytically inactive nonstoichiometric TiO<sub>2</sub>-xNx structures were deposited. The absence of semiconductive properties of the films obtained at the low pressures is a direct evidence of no anatase formation and, respectively, their photocatalytic performance remained at the level of blank experiments.

It can be suggested that carbon and hydrogen radicals/atoms forming as a result of laser action react with oxygen species causing the subsequent oxygen substitution by nitrogen atoms.

This mechanism is supported by the XPS evidence, according to which the intensity of N–Ti peak at 395.9 eV is lower for the samples synthesized in a pure N<sub>2</sub> atmosphere. Thus, the effective incorporation of substitutional nitrogen in oxide matrix can be caused by a direct interaction of carbon or hydrogen atom with oxygen species during PLD resulting in an oxygen deficient lattice, taking into account that pure methane used in PLD prevents anatase formation providing oxygen atoms deficiency. At high pressure, a number of collisions between C or H species and ablated oxygen atoms are less probable owing to the screening effect of other atoms/species (**Figure 7a**). When pressure is decreased, the deposition rate is enhanced in addition to much higher probability for carbon/oxygen and hydrogen/oxygen interactions (**Figure 7b**). This can result in the higher efficiency of Ti–N as compared with Ti–O fragments formation.

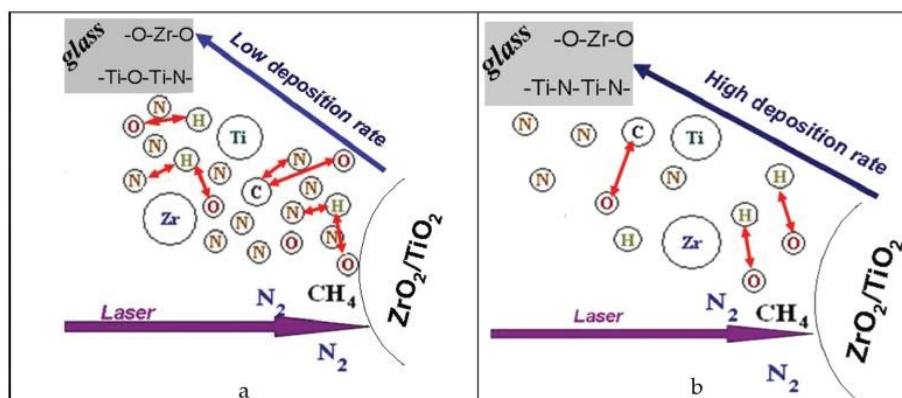


**Figure 7.** Schematic representation of pulse laser deposition in a mixture of N<sub>2</sub>/CH<sub>4</sub> at 100 Pa (a) and 3 Pa (b).

As seen from **Figure 8**, the percentage of reduced dichromate ions under UV light is correlated with the contributions of N1s at 395.8 eV which is in turn dependent on the zirconia content.

The ratio of line intensities of N1s at 395.8 eV to Ti2p<sub>3/2</sub> at 457.5 eV is pointing to the large number of O–Ti<sup>3+</sup>–N bonds with the increase of ZrO<sub>2</sub> contents. It is obvious that photocatalytic activity under UV light strongly depends on the efficiency of substitutional nitrogen incorporation inside titania matrix. The high ZrO<sub>2</sub> content (50%) induces the deceleration of anatase crystallization rate leading to the activity decrease, while a much lower zirconia amount (2.5 and 5%) is still not enough to stimulate an appropriate quantity of substituted nitrogen embedded in titania matrix. The correlation between the zirconia content and the efficiency of substitutional N incorporation is established. The distortion of Ti<sup>4+</sup>O<sub>2</sub> lattice with the advent of Ti<sup>3+</sup> states occurred due to the larger radius of zirconium ions (R<sub>Zr<sup>4+</sup></sub> = 0.720 Å vs. R<sub>Ti<sup>4+</sup></sub> = 0.650 Å). The relative high stability of Ti<sup>3+</sup> states is assigned to the presence of Zr<sup>4+</sup> ions.

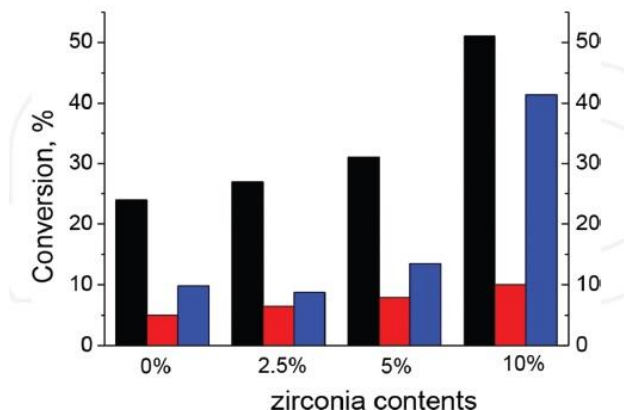


**Figure 8.** Influence of zirconia contents in  $(xZr)TiN5C1/100$  films on the photocatalytic conversion under UV (black column), ratio of N1s at 395.8 eV to Ti2p at 457.5 eV (red column) and N1s at 395.8 eV to total N1s (blue column).

In general, the low photocatalytic efficiency is explained by the limited photo-excitation of electrons in the intragap localized states, the very low mobility of photogenerated holes, and the high recombination rate due to the creation of oxygen vacancies by doping. Hence, the photoreactivity of doped TiO<sub>2</sub> appeared to be a complex function of the doping agent concentration, the energy level of doping agent within the TiO<sub>2</sub> lattice, their d electronic configurations, the distribution of doping agent, the electron donor concentrations, and light intensity.

The debates concerning the preferred N substitutional or interstitial sites which induce the highest photocatalytic action is still alive in the literature. Our investigation suggests that the substitutional nitrogen (Ti–N) that belongs to XPS lines at 395.2–395.8 eV is basically responsible for the observed photoactivity. Additionally, it can be proved by the next two observations. (i) The peak at 397.8 eV has the negligible relative intensity (2.8%) for most active **10ZrTiN5C1/100**, and (ii) the peaks in the range of 398–401 eV are observed for the other samples with low reactivity. We also underline that Ns species with 395.2–395.8 eV binding energy are responsible for bandgap narrowing or formation of intragap localized states of the doping agent within bandgap. It is pointed that the bandgap energy values are sharply declined when the relative intensity of this XPS peaks is increased, while no dependence between 397.8 or 398–401 eV peaks and E<sub>bg</sub> is observed. PLD synthesis of TiO<sub>2</sub> films in N<sub>2</sub>/CH<sub>4</sub> atmosphere not only leads to nitrogen incorporation but also to the formation of defects including oxygen vacancies and Ti<sup>3+</sup> states which are all contributing to light absorption.

#### D. Conclusions

1. The studies performed in the period 2015-2016 was concerning TiO<sub>2</sub>.
2. O atentie speciala a fost acordata proceselor de sinteza prin tehnici laser pulsate: PLD, MAPLE si C-MAPLE. Special attention was granted to the synthesis by pulsed laser techniques: PLD, MAPLE and C-MAPLE.
3. The properties of the simple and doped TiO<sub>2</sub> layers were studied together with their potential to be used as sensors and for the laser catalysis.
4. There were elaborated theoretical models which offered the possibility to evaluate the main physical phenomena related to the interaction between the laser radiation and TiO<sub>2</sub> layers. Also, numerical simulations were performed on complex structures.
5. Spectacular results with international recognition were obtained in the case of laser catalysis as an effect to natural light exposure. The conversion to benign compounds of some salts of high toxicity were evidenced together with an spectacular effect upon the decontamination of the highly contaminated media.
6. All the investigations concretized in international scientific collaborations with partners from Italy, Republic of Moldova, Ukraine and Serbia.

Date,

December2, 2016

Project Director  
Prof. Dr. Ion N. Mihailescu